ACS APPLIED MATERIALS & INTERFACES

Research Article

www.acsami.org

Amphiphilic Thiol Functional Linker Mediated Sustainable Anti-Biofouling Ultrafiltration Nanocomposite Comprising a Silver Nanoparticles and Poly(vinylidene fluoride) Membrane

Sung Yong Park,[†,∥] Jae Woo Chung,[‡,∥] Young Kee Chae,[§] and Seung-Yeop Kwak*[,†]

[†]Department of Materials Science and Engineering, Seoul National University, 599 Gwanak-ro, Gwanak-gu, Seoul 151-744, Korea

[‡]Department of Organic Materials and Fiber Engineering, Soongsil University, 369 Sangdo-ro, Dongjak-gu, Seoul 156-743, Korea

[§]Department of Chemistry and Recombinant Protein Expression Center, Sejong University, 98 Gunja-Dong, Gwangjin-Gu, Seoul 143-747, Korea

Supporting Information

ABSTRACT: We develop sustainable anti-biofouling ultrafiltration membrane nanocomposites by covalently immobilizing silver nanoparticles (AgNPs) onto poly(vinylidene fluoride) (PVDF) membrane mediated by a thiol-end functional amphiphilic block copolymer linker. Field emission scanning electron microscopy (FE-SEM) and energy-dispersive X-ray spectroscopy (EDXS) measurements reveal that the AgNPs are highly bound and dispersed to the PVDF membrane due to the strong affinity of the AgNPs with the thiol-modified block copolymeric linkers, which have been anchored to the PVDF membrane. The membrane performs well under water permeability and particle rejection measurements, despite the high deposition of AgNPs on the surface of membrane. The Ag-PVDF membrane nanocomposite significantly inhibits the growth of bacteria on the membrane surface, resulting in enhanced anti-biofouling property. Importantly, the AgNPs are not released from the membrane surface due to the robust covalent bond between the AgNPs and the thiolated PVDF membrane. The stability of the membrane nanocomposite ensures a sustainable anti-biofouling activity of the membrane.

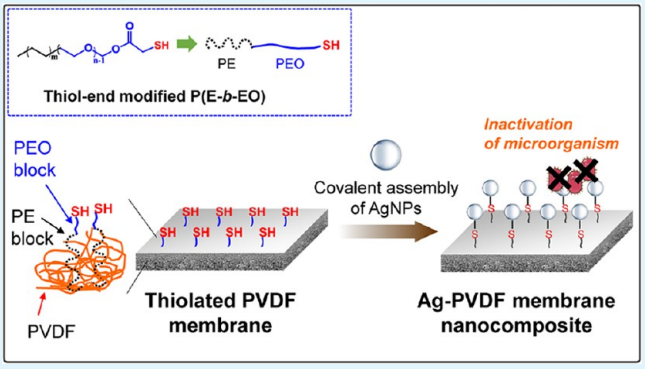

KEYWORDS: *anti-biofouling, covalent bonding, PVDF membranes, silver nanoparticles (AgNPs), thiol functional amphiphilic linker*

INTRODUCTION

The lack of clean water is a serious problem in many countries. According to estimations from the World Health Organization (WHO) and the United Nations Children's Fund (UNICEF), more than 884 million people lack hygienic drinking water.[1] Significant efforts have been applied toward producing clean water by purifying contaminated water. Membrane filtration techniques offer a relatively cost-effective approach to the production of high-quality purified water; however, the process tends to clog the membranes by depositing the retained organic materials, inorganic materials, and microorganisms on the membrane surface or into the membranes pores.[2] This phenomenon, that is, membrane fouling, deteriorates the membrane performance and increases the maintenance costs by requiring regular membrane cleaning or replacement.[3,4] Especially, membrane biofouling by microorganism is a major obstacle to successful membrane operation because the microorganisms that accumulate on a membrane surface not only grow over time, but also they tend to form a dense biofilm that blocks membrane function.[5,6]

To solve the membrane biofouling problems, a variety of reactive functional materials, such as hydrophilic,[2,7−9] charged,[10−12] photocatalytic,[13−16] or biocidal materials,[17−21] have been introduced into the ultra- and microfiltration membranes. These materials can reduce membrane biofouling by adhesion inhibition (hydrophilic, charged matters) of hydrophobic foulants or decomposition (biocidal, photocatalytic, positively charged matters) of microbial foulants. Although these material's properties endow good antifouling properties to the water treatment membrane, a number of limitations have been associated with these materials, including stability (autoxidation), pH dependence (losing their charge by deprotonation), and membrane degradation.[22−24] Exceptionally, among the biocidal materials, silver nanoparticles (AgNPs), display strong inhibitory and a biocidal properties against a variety of microorganism types with long time periods.[24−28] Significant efforts have been devoted to introducing AgNPs into polymeric membrane substrates to form AgNP/membranes nanocomposite. AgNP/membranes nanocomposite are usually prepared through a nonsolvent induced phase

Received: July 16, 2013
Accepted: October 21, 2013
Published: October 21, 2013

separation (NIPS) process using an AgNPs-included dope solution.[17,19−21] AgNPs have also been coated directly onto polymer membrane substrates to form AgNP/membranes nanocomposite;[18] however, the practical utility of these methods has been limited by the low efficiency of AgNP deposition onto the membrane surfaces. Furthermore, the immobilized AgNPs can be released (or leached) from the membranes owing to the lack of interaction between AgNP and membrane. Indeed, Alvarez and coworkers reported that the AgNPs which were located on the membrane surface were readily removed during water filtration process.[17] The unwanted loss of the AgNPs from the membrane brings about the deterioration in the desired properties such as an anti-biofouling property and a membrane life time. Most problematic of all, the AgNPs released from the membrane can penetrate easily into the human body, can produce cell damage and cancer.[29−31]

Recently, Mauter and coworkers described the preparation of AgNPs/membrane nanocomposites in which the AgNPs were electrostatically assembled on the membrane. The membrane was prepared by means of the assembly between the AgNPs encapsulated with the positively charged polyethyleneimine (PEI) and the polysulfone (PSF) membrane functionalized with the negative charged carboxylic acid.[32] Electrostatic interactions were useful for depositing the AgNPs on the membrane substrate; however, the AgNPs were eventually released from the membrane due to the weakness of the electrostatic attraction between the AgNPs and the membrane.[17] Stable and robust bonds between the AgNPs and the membrane are important for ensuring the preparation of safe, ecofriendly, stable, anti-biofouling, and high-efficiency membranes. We have described a metal−cellulose fabric nanocomposite in which silver or palladium nanoparticles are covalently assembled onto a thiolated cellulose fabric.[33] The thiol group in the thiolated cellulose formed a robust covalent bond with the Ag atoms on the surface of the metal nanoparticles, thereby significantly reducing the number of metal nanoparticles released from the fabric during washing. Despite the utility of the metal−sulfur covalent bond, to the best of our knowledge, no reports have described the covalent assembly of AgNPs on a water treatment membrane using the metal−sulfur bond.

Here, we describe the AgNP-poly(vinylidene fluoride) (Ag-PVDF) membrane nanocomposites having a sustainable anti-biofouling property through the covalent assembly of the AgNPs onto the PVDF membrane surface via a thiol end-functionalized amphiphilic block copolymeric linker. To this end, the thiol end-functionalized amphiphilic block copolymer as a covalent linker between the AgNPs and the membrane was physically anchored onto the membrane via hydrophilic−hydrophobic phase recognition of the amphiphilic linkers during the NIPS membrane fabrication process, resulting in the thiolated PVDF membrane. AgNPs then covalently bound to the thiolated PVDF membrane via a simple impregnation process. Surprisingly, the resulting Ag-PVDF membrane nanocomposite did not release detectable amounts of AgNPs from the membrane, and the membrane displayed excellent anti-biofouling property. This makes them tremendously attractive in applications ranging from high-efficiency membrane to ecofriendly water purification systems.

MATERIALS AND METHODS

Materials. Polyvinylidene fluoride (PVDF, M_w = 570 000 g mol^{-1}) was supplied by Solvay Chemicals. Silver nitrate ($AgNO_3$, 99%), trisodium citrate ($C_6H_5Na_3O_7$, analytic grade), sodium borohydride ($NaBH_4$, 98.5%), polyethylene-*block*-polyethylene glycol (P(E-*b*-EO), M_n = 2250 g mol^{-1}; PEO, 80%), toluene (C_7H_8, 99.5%), and mercaptoacetic acid ($C_2H_4O_2S$, 98%) were purchased from Sigma-Aldrich. *N*,*N*-Dimethylacetamide (C_4H_9NO, 99%) was purchased from Tokyo Chemical Industry (TCI). Polyvinylpyrrolidone (PVP, M_w = 40 000 g mol^{-1}) and diethyl ether ($C_4H_{10}O$, analytic grade) were supplied by Daejung Chemicals & Metals. All chemicals were used as received without further purification. The aqueous solutions were prepared from deionized (DI) water having a resistivity exceeding 18.0 MΩ cm.

Preparation of the Thiol-Modified Amphiphilic Block Copolymer Linker. The linker used for the covalent assembly of AgNPs with the PVDF membrane was prepared by converting the hydroxyl group of the P(E-*b*-EO) to a thiol group through an esterification reaction using mercaptoacetic acid. A 11.3 g sample of P(E-*b*-EO) was dissolved in 50 mL of dry toluene at 80 °C. After complete dissolution of the P(E-*b*-EO), the mixture containing 1.38 g of mercaptoacetic acid and 0.5 mL of concentrated sulfuric acid was slowly added dropwise to the P(E-*b*-EO) solution. The solution was vigorously stirred at 110 °C for 2 h. The solution was then dropped into cold diethyl ether with vigorous stirring, and the crude product was filtered out. To remove the unreacted reactants, the crude product was washed several times with diethyl ether and filtered. The final product was dried in a vacuum at room temperature for overnight. The thiol-modified P(E-*b*-EO) was characterized by Fourier-transform infrared spectroscopy (FT-IR, Thermo Scientific Nicolet 6700 FT-IR spectrometer) with a spectral resolution of 4 cm^{-1} over the range 4000−400 cm^{-1} and by ^{1}H nuclear magnetic resonance (^{1}H NMR, Bruker AVANCE 600) spectroscopy using $CDCl_3$ as a solvent.

Preparation of the Thiolated PVDF Membrane. The thiolated PVDF membrane was prepared via hydrophilic−hydrophobic phase recognition between the thiol-modified amphiphilic linker and the PVDF polymer during a NIPS process. The membrane dope solution was prepared by dissolving 15 wt % PVDF, 5 wt % PVP, and 0.75−2.25 wt % thiol-modified P(E-*b*-EO) (5−15 wt % per PVDF raw material) in a DMAc solution at 40 °C for overnight using a mechanical stirrer. The dope solution was put in an oven at 40 °C for 2 h to remove any bubbles. The dope solution was cast onto a glass plate using a 200 μm casting applicator, and the cast film was immediately immersed in DI water, which acted as a nonsolvent, to produce a PVDF flat sheet membrane incorporating the linkers having thiol functional groups. The thiolated membrane was then carefully rinsed with DI water to remove the solvent, pore-forming agent, and unanchored linker. The thiolated PVDF membrane was denoted PVDF-SH*X*, where *X* indicates the weight percentage of the thiol-modified P(E-*b*-EO) relative to the PVDF in the dope solution. For comparison, we prepared a neat PVDF membrane using the protocol described above except that the thiol-modified P(E-*b*-EO) was not added. All membranes were stored in DI water prior to use.

Preparation of the AgNP-Covalently Assembled PVDF Membrane Nanocomposite. The colloidal AgNPs were synthesized according to previously reported protocols.[34,35] Briefly, 20 mL of a 1 mM $AgNO_3$ aqueous solution was mixed with an equal volume of a 1 mM trisodium citrate solution. A 0.6 mL volume of 0.1 M $NaBH_4$ solution was quickly injected into the $AgNO_3$/trisodium citrate mixture with vigorous stirring at room temperature. The color of the solution immediately changed from dark gray to yellow, indicating the successful formation of AgNPs. The size of as-synthesized AgNPs was ca. 5−8 nm (see Figure S1 in the Supporting Information). The AgNPs were covalently bound to the thiolated PVDF membrane by immersing a sample of the prepared thiolated PVDF membrane (10 × 8 cm^2) into the colloidal AgNP aqueous solution under mildly basic conditions. The solution was then agitated gently at room temperature in an orbital shaker for 1 day. The specimen was then carefully rinsed several times with DI water to remove loosely bound AgNPs, and the sample was stored in a DI water bath prior to use. The AgNP−PVDF

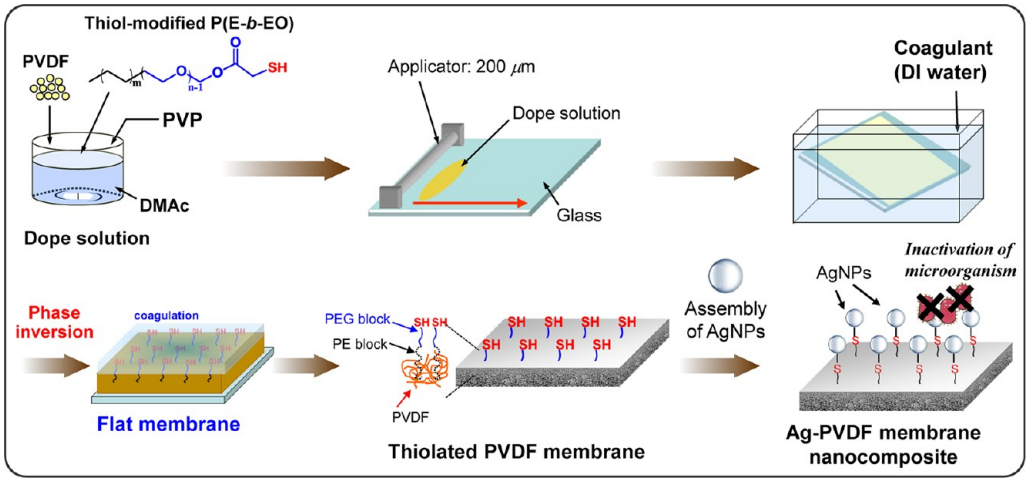

Figure 1. Schematic illustration of the procedure for the formation of the silver nanoparticles covalently assembled on the PVDF membrane (Ag-PVDF membrane nanocomposite).

membrane nanocomposite was denoted Ag-PVDF. The overall procedure used to prepare the Ag-PVDF membrane nanocomposite is schematically illustrated in Figure 1. For comparison, the neat PVDF membrane was treated with the AgNP colloid in the same manner used for the production of Ag-PVDF. The neat PVDF membrane into which noncovalently bound AgNPs had been introduced was denoted Ag/PVDF.

Characterization of the Membrane. The thiolated PVDF membrane was analyzed by attenuated total reflection Fourier-transform infrared (ATR FT-IR, Thermo Scientific Nicolet 6700 FT-IR spectrometer) spectroscopy with a spectral resolution of 4 cm^{-1} over the scan range from 4000 to 650 cm^{-1}. The surface and cross-sectional morphologies of the membranes were observed by field-emission scanning electron microscopy (FE-SEM, Carl Zeiss SUPRA 55VP, JEOL 7800F) and energy-dispersive X-ray spectroscopy (EDXS, Bruker X-flash-4010). The samples used for FE-SEM imaging were coated with a thin Pt layer (ca. 20 nm thick). The Ag loading in the Ag-PVDF was determined using inductively coupled plasma atomic emission spectrometry (ICP-AES, PerkinElmer Optima-4300 DV) with an argon plasma source operated at 6,000 K. The pure water permeability (PWP) of each membrane was measured using an Amicon 8050 dead-end stirred cell (Millipore Corp.) connected to a pressure vessel filled with DI water. The PWP was measured continuously by collecting the permeate on an analytic mass balance (CAS CUW 420H) at constant pressure (1 bar), and the value was calculated using the following eq 1,

$$\mathrm{PWP} = Q/(tA\Delta P) \quad (1)$$

where Q is the volume (L) of the permeate, t is the filtration time (h), A is the effective membrane area (m^2), and ΔP is the transmembrane pressure (bar).

The membrane pore size was analyzed by filtering an aqueous suspension of polystyrene (PS) latex beads (diameter: 0.06 μm and 0.1 μm) and γ-globulin (diameter: 20−30 nm at pH 7) through the membrane. The rejection value of each particle was calculated using the following eq 2,

$$R\ (\%) = \left(1 - \frac{C_p}{C_f}\right) \times 100 \quad (2)$$

where R (%) is the rejection percentage of these particles and C_p and C_f are the particle concentrations in the permeate and feed solutions, respectively. The particle concentrations in the feed (C_f) and permeate (C_p) solutions were determined using standard concentration curves for the PS latex bead and the γ-globulin, plotted using the turbidity value of each PS latex particle and the UV absorbance intensity at λ_{max} (279 nm) of γ-globulin, respectively. The concentration of each filtrate was determined using a linear regression of the standard curves. The turbidity of the PS latex suspended solution and the UV absorbance of the γ-globulin suspensions were measured using a turbidity analyzer (HACH 2100 AN) and a UV-visible spectrometer (PerkinElmer Lambda 25), respectively.

Test of the AgNP Release from the Membrane. The binding stability between the AgNPs and the membrane was tested by conducting a AgNP release test in which DI water was continuously filtered through the Ag-PVDF membrane nanocomposite (effective membrane area: 13.4 cm^2) using the Amicon dead-end stirred cell. The degree of AgNP release from the membrane was quantitatively analyzed by evaluating the concentration of Ag in the filtrate using ICP-AES. The amount of Ag present on the membrane surface was analyzed by X-ray photoelectron spectroscopy (XPS), and the patterns were recorded using a Kratos AXIS-HSi spectrometer featuring a monochromatic Mg Kα X-ray source operated at 10 mA.

Evaluation of the Biofouling Resistance. Membrane anti-adhesion and biofouling resistance tests were conducted using an aqueous suspension of *Escherichia coli*. The *E. coli* TOP10 strain (purchased from Invitrogen) was first cultured in a (250 mL) flask in Luria-Bertani (LB) broth (1% bactotryton, 0.5% yeast extract, 1% NaCl) in a 37 °C incubation shaker for 20 h to obtain a suspension of stationary phase bacteria (~10^9 CFU/mL). Prior to the bacterial adhesion and filtration experiments, all membranes were rinsed with 70% ethanol aqueous solution for 30 minutes and then incubated for 30 minutes in each of a series diluted aqueous ethanol solutions (50, 25, 0% aqueous ethanol solution) to remove ethanol from the membrane. The bacteria adhesion to the resulting membrane surface was evaluated by incubating the stationary phase bacteria in the presence of neat PVDF and Ag-PVDF membranes (1 × 1 cm^2) in a 37 °C incubation shaker for 4 h. The membranes were then removed from the *E. coli* suspension solutions and carefully rinsed several times with phosphate buffered saline (PBS). The bacteria that adhered to the membrane were observed by FE-SEM imaging. Prior to FE-SEM observation, the bacteria adhered to the membrane were fixed in a 4% (v/v) glutaraldehyde solution,[36] and the resulting membranes were dehydrated with ethanol and dried at room temperature.

The resistance due to biofouling during filtration was assessed by conducting a filtration test using *E. coli* as a biofoulant. The membranes were inoculated by applying 6 mL of an *E. coli* suspension solution (~10^7 CFU/mL) to the membrane using a vacuum filter cell. LB broth solution (concentration: 0.5 g/L) was then filtered over the inoculated membrane for 24 h to provide a feed solution. The feed solution temperature was kept at 25 °C using a laboratory-grade constant temperature water bath. The flux was recorded using an analytic mass balance. After 24 h, the membrane was rinsed with DI water for 10 minutes to remove unattached *E. coli* and its byproducts from the membrane surface. The flux recovery was assessed by flushing the membrane with DI water using the filtered cell and re-measuring

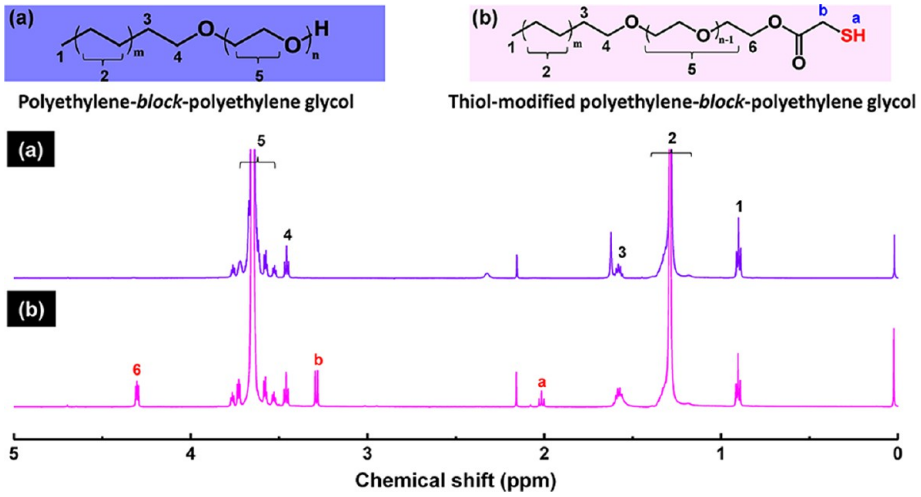

Figure 2. ^{1}H NMR spectra of (a) the polyethylene-*block*-polyethylene glycol and (b) the thiol-modified polyethylene-*block*-polyethylene glycol copolymer. The degree of thiol-modification was calculated from the ratio of the integrals over 4 and 6 in the ^{1}H NMR spectrum of the thiol-modified polyethylene-*block*-polyethylene glycol.

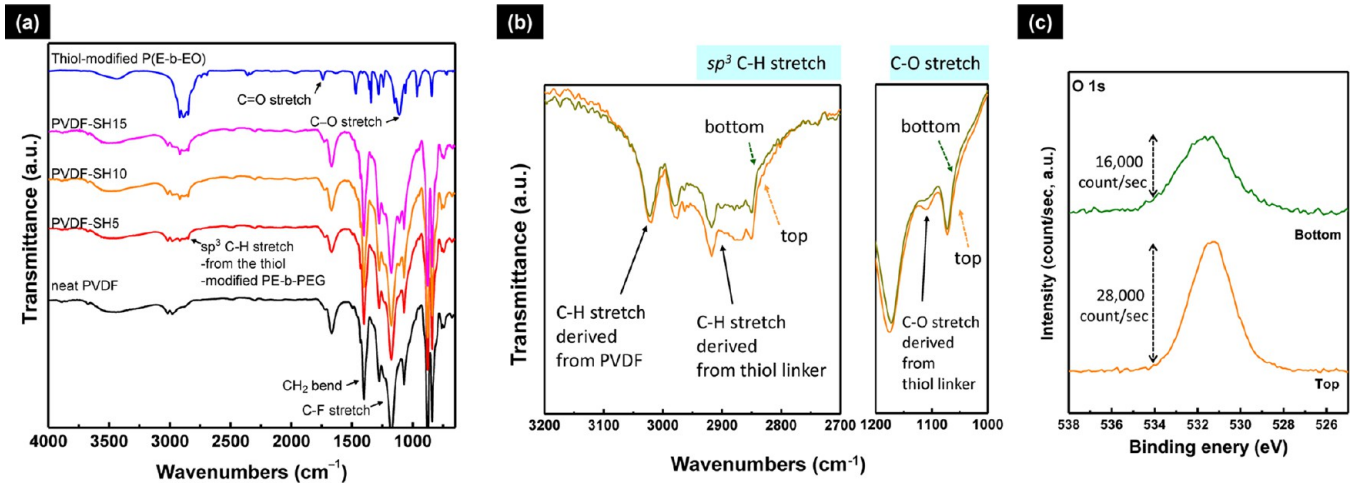

Figure 3. (a) FT-IR spectra of the neat PVDF membrane, thiolated PVDF membranes, and the thiol-modified amphiphilic copolymer linker. (b) ATR FT-IR spectra of both surfaces (top and bottom) of the thiolated PVDF membrane, collected over the range 3200−2700 cm^{-1} and 1200−1000 cm^{-1}, corresponding to the C−H and C−O stretches of the linker, respectively. (c) XPS spectra of O 1s of both top and bottom surfaces.

the PWP. The filtration test results are reported in terms of the normalized flux, which was calculated using the following eq 3,

$$N = F_t/F_i \quad (3)$$

where N is the normalized flux, F_t is the flux value, and F_i is the initial flux value. Equations 4−6 give the decrease in total flux due to membrane fouling:

$$r_t(\%) = (1 - N_f) \times 100 \quad (4)$$

$$r_{rev}(\%) = (N_w - N_f) \times 100 \quad (5)$$

$$r_{ir}(\%) = (1 - N_w) \times 100 \quad (6)$$

where r_t, r_{rev}, and r_{ir} are the degree of decrease in the total, reversible, and irreversible fluxes, respectively. N_f and N_w are the normalized flux values of the fouled membrane and pure water flushed membrane, respectively.

RESULTS AND DISCUSSION

Thiol-Modified Amphiphilic Block Copolymer Linker. The thiol-modified amphiphilic block copolymer linker was prepared via an esterification reaction between the hydroxyl end group of P(E-*b*-EO) and the mercaptoacetic acid. The reaction progress was monitored by FT-IR spectroscopy (see Figure S2 in the Supporting Information). The IR transmittance spectrum of the thiol-modified P(E-*b*-EO) was indistinguishable from that of the neat P(E-*b*-EO), with the exception of a peak consistent with a carbonyl stretch at 1739 cm^{-1}. The carbonyl stretching for the thiol-modified P(E-*b*-EO) was observed to the higher wavenumber than that for mercaptoacetic acid (1716 cm^{-1}). The peak shift was attributed to the esterification reaction between the hydroxyl group of the P(E-*b*-EO) and mercaptoacetic acid, which further indicates that the thiol functional group was successfully introduced onto the end of the P(E-*b*-EO) molecule via an esterification reaction between the hydroxyl end group of the P(E-*b*-EO) and the mercaptoacetic acid. In addition to FT-IR studies, ^{1}H NMR measurements of the thiol-modified P(E-*b*-EO) were collected to quantify the degree of thiol modification. As shown in Figure 2, new peaks appeared at 4.3, 3.3, and 2.0 ppm in the thiol-modified P(E-*b*-EO), which corresponded to $-CH_2OOC-CH_2-SH$ (4.30 ppm), $-CH_2OOC-CH_2-SH$ (3.29 ppm), and $-CH_2OOC-CH_2-SH$ (2.01 ppm), and were attributed to the

dx.doi.org/10.1021/am402855v | ACS Appl. Mater. Interfaces 2013, 5, 10705−10714

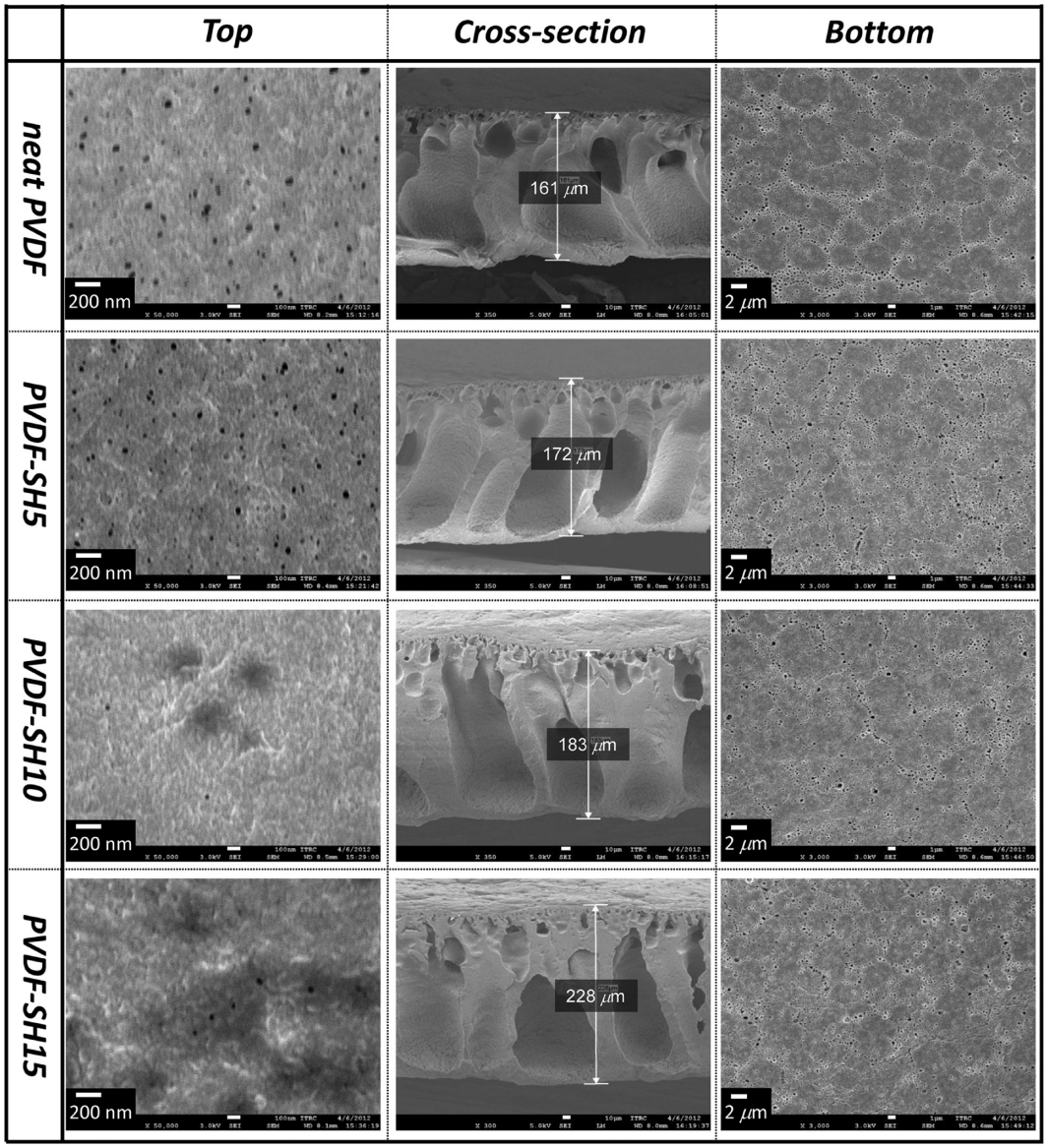

Figure 4. Top surface (left), cross section (center), and bottom surface (right) morphologies of the neat (1st line) and thiolated (2−4 lines) PVDF membranes, collected using FE-SEM observation.

substitution of the P(E-*b*-EO) hydroxyl group with the thiol functional group. The degree of thiol modification was calculated from the ratio of the integrals of the PEO methylene protons (at 4.30 ppm) adjacent to the ester functionality and the PE methylene protons (at 3.46 ppm) adjacent to the ether functionality, assigned as 6 and 4 in Figure 2, respectively. The calculated degree of thiol modification in the thiol-modified P(E-*b*-EO) was 99%, indicating that nearly all of the P(E-*b*-EO) hydroxyl end groups had been converted to thiol groups and that the preparation of the thiol-modified amphiphilic block copolymer linker was successful.

Thiolated PVDF Membrane. The thiolated PVDF membrane was fabricated through a non-solvent induced phase separation (NIPS) process of the PVDF dope solution including the varied amount of the amphiphilic thiol-modified P(E-*b*-EO) linker. Figure 3 shows the ATR FT-IR transmittance patterns of the thiol-modified linker, the neat PVDF membrane, and the thiolated PVDF membranes. As shown in Figure 3a, the IR bands corresponding to the sp^3 CH stretch of the linker (between 2850 and 2920 cm^{-1}) were more pronounced in the thiolated PVDF membranes prepared with a larger amount of the linker in the PVDF dope solution. The C−O stretch at 1150 cm^{-1} in the FT-IR spectra of the thiolated PVDF membranes, which was attributed to the PEO ether linkage in the linker molecule, gradually grew in as the amount of linker in the dope solution increased. These results indicate that the linkers have been successfully incorporated into the membrane. The mechanism by which the linkers were introduced into the membrane during the NIPS process was investigated by analyzing the IR transmittance through the top and bottom surfaces of the thiolated PVDF membrane. Here, the top surface corresponds to the water contact side and the bottom surface corresponds to the glass contact side. As shown in Figure 3b, the intensity of the sp^3 CH stretch (between 2850 and 2920 cm^{-1}) for the top surface was higher than that for the bottom surface. The C−O stretch at 1110 cm^{-1} was also slightly stronger for the top surface than for the bottom surface. In addition, the XPS spectra of O 1s (Figure 3c) showed the difference intensity and concentration of oxygen between top and bottom surfaces of the thiolated PVDF membrane. Oxygen

Table 1. PWP Values Obtained from the neat PVDF and the Thiolated PVDF Membranes with Different Loadings of the Thiol-Modified Linker

		thiolated PVDF		
sample name	neat PVDF	PVDF-SH5	PVDF-SH10	PVDF-SH15
PWP (L m^{-2} h^{-1} bar^{-1})	1742 ± 35	1696 ± 65	418 ± 41	345 ± 24

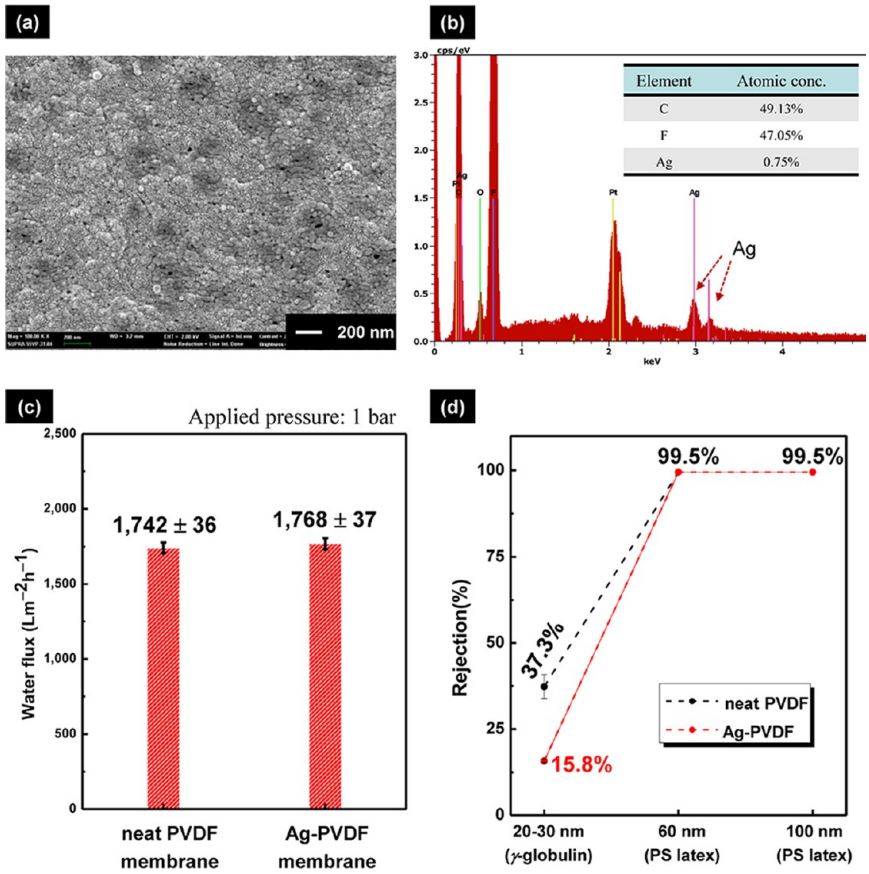

Figure 5. Characteristics of the Ag-PVDF: (a) Top surface morphology observed by FE-SEM and (b) chemical composition of the membrane surface obtained by EDXS. Membrane performances of the neat PVDF membrane and the Ag-PVDF membrane nanocomposite. (c) Pure water permeability and (d) rejection of the standard sized particles (γ-globulin, 0.06 and 0.1 μm polystyrene latex beads). The bars with the standard deviation represent the average of three filtration results.

species in the thiolated PVDF membrane were derived from the PEO block. Therefore, the degree of surface thiol functionalization can be calculated by analysis of oxygen amount in the membrane surface. From the XPS spectra, we found the intensity of O 1s of the top surface (3.45 wt %) was much bigger than that of the bottom surface (1.37 wt %). These oxygen amounts can be converted into the amount of sulfur element, and the sulfur elements calculated from the amount of oxygen were 0.16 wt % for the top surface and 0.06 wt % for the bottom surface. This reveals that the thiol linker were located at the top surface ca. 2.5 times more than at the bottom surface. As a result, the silver loading mount on the top surface were much higher than that on the bottom surface (see Figure S4 in the Supporting Information). Thus, the combined results of the ATR FT-IR and the XPS suggest that the thiol-modified P(E-*b*-EO) linker migrated toward the top surface during the NIPS process due to the hydrophilic affinity of the PEO segment in the linker with the water contacted with the top surface of the membrane. In water, the hydrophilic–hydrophobic phase recognition of the linker during the membrane formation most likely exposed the thiol functional group attached to the end of the PEO segment of the linker to the membrane surface, whereas the hydrophobic PE moiety was inserted into the consolidated hydrophobic PVDF layer. These migrations resulted in a self-assembled thiol-functionalized PVDF membrane. Perfect phase separation by the amphiphilic linker was not likely to occur during the PVDF consolidation process in water, as the NIPS process was far too rapid to provide sufficient time for the linker to fully undergo phase separation. Some of the linker may remain present on the inside of the membrane. Nevertheless, the IR spectra from the top and bottom surfaces of the thiolated PVDF membrane show that the linker was mainly present near the membrane surface, thereby allowing the thiol functional linker on the PVDF membrane to covalently bond to the AgNPs.

The effects of the linker on the PVDF membrane structure were characterized by measuring the morphologies of the thiolated PVDF membranes prepared with various amounts of the linker, that is, neat PVDF (PVDF-SH0), PVDF-SH5, PVDF-SH10, and PVDF-SH15 membranes. The PWP values of each membrane were also measured. FE-SEM (Figure 4) showed that the neat and thiolated PVDF membranes displayed

similar morphologies typically observed in asymmetric membranes composed of a dense top layer and a porous bottom layer. The thiolated PVDF membrane thickness was found to increase and the number of pores on the top surface layer decreased as the amount of linker in the membrane increased. Indeed, as listed in Table 1, the thiolated PVDF membranes produced from the dope solution containing more than 1.5 wt % linker in the dope solution, that is, PVDF-SH10 and PVDF-SH15, exhibited the most dramatic decreased in the PWP values compared to the neat PVDF membrane due to a higher membrane thickness and a reduced number of surface pores. This can be attributed to the presence of PE moiety in the linker. Basically, PE moiety is insoluble in DMAc solution. Thus, excess of PE moiety can reduce the thermodynamic stability of the membrane dope solution and inhibit the pore formation in the PVDF membrane. On the other hand, the PWP and morphology of the PVDF-SH5 membrane were nearly indistinguishable from the corresponding properties of the neat PVDF membrane. These results clearly demonstrated that the membrane formation was not affected by the presence of less than 0.75 wt % linker in the dope solution. We therefore selected the PVDF-SH5 membrane for the preparation of the Ag-PVDF membrane nanocomposite.

Ag-PVDF Membrane Nanocomposite. Thiol functional groups form strong coordination bonds with noble metals, for example, Ag and Au, that have a relatively large ionic radius and a low oxidation state. According to Pearson's hard and soft acids and base (HSAB) theory,[37] the sulfur atom in a thiol group and a noble metal tend to share the valence electrons to form a covalent bond. Alkyl sulfide anions, in particular, which form through the removal of a proton from a thiol group, have a stronger affinity toward these metals than a thiol group. Mildly basic conditions, therefore, favored deprotonation of alkyl thiol and the formation of covalent bonds between the colloidal AgNPs and the thiolated membrane (PVDF-SH5), when we immersed PVDF-SH5 membrane in the colloidal AgNP solution under the mildly basic condition. As anticipated, the color of the membrane changed from white to reddish-yellow (Figure S3, Supporting Information), indicating that the AgNPs were successfully immobilized on the surface of the membrane due to the formation of strong sulfur−metal bonds mediated by the thiol-modified linker embedded in the membrane, yielding the self-assembled AgNPs-PVDF (Ag-PVDF) membrane nanocomposites. Figure 5a and b shows the surface morphology and elemental analysis of the Ag-PVDF membrane nanocomposite measured by FE-SEM and EDXS, respectively. The FE-SEM image (Figure 5a) showed that the spherical AgNPs were directly attached to the surface of the membrane. The EDXS spectra of the Ag-PVDF membrane nanocomposite (Figure 5b) distinctly revealed that the AgNPs were present on the surface of the Ag-PVDF membrane nanocomposite. As can be seen Figure 5a, the size of attached AgNP on the membrane surface is seem to increase compared to the as-synthesized AgNP (below 10 nm). This can be attributed to a breakdown of the electronically repulsive stabilizing structure of AgNP by introducing the covalent bond at the nanoparticle surface and a subsequent partial aggregation between AgNPs on the surface of the membrane.[38] The extent of AgNP loading in the Ag-PVDF membrane nanocomposite was evaluated using ICP-AES to quantitatively analyze the effects of the thiol functionality in the membrane on the deposition of AgNPs to the membrane. The Ag elemental loading was 10 266 mg kg^{-1} in the Ag-PVDF membrane nanocomposite. By contrast, the Ag/PVDF membrane nanocomposite prepared without the thiolated linkers yielded a Ag elemental loading that was approximately 5 times lower (2,124 mg kg^{-1}) than that of the Ag-PVDF membrane nanocomposite. These results indicate that the presence of the thiolated linker in the membrane played a key role in stabilizing the AgNPs on the membrane surface.

The PWP value and rejection properties of the Ag-PVDF membrane nanocomposite were characterized as a measure of the membrane performance. Figure 5c shows that the Ag-PVDF membrane nanocomposite (1768 ± 37 L m^{-2} h^{-1}) had a PWP value comparable to that of the neat PVDF membrane (1742 ± 36 L m^{-2} h^{-1}), indicating that the two membranes provided similar water treatment efficiencies. The rejection properties of the two membranes were similar as well. Both membranes yielded a high rejection (exceeding 99%) of 0.1 and 0.06 μm PS latex particles, although the Ag-PVDF membrane nanocomposite exhibited a slightly lower rejection of 20−30 nm γ-globulin relative to the neat PVDF membrane (Figure 5d). This means that the largest surface pore size in both membranes appeared to be within the range 30−60 nm. It is seemed that the introduced AgNPs to the membrane did not reducing the surface porosity because the small sized AgNPs can pass through surface pore then bind a highly porous support layer rather than clogging surface pore. Thus, the assembly of AgNPs to the PVDF-SH5 membrane did not significantly affect the structure and performance of the membrane, which anticipate that the Ag-PVDF membrane nanocomposite well apply to real water purification system.

Release of Ag from the Membrane. The stable and robust bond between the AgNPs and the membrane is important for ensuring the maintenance of anti-biofouling performance for high-efficient and eco-friendly membrane system. The quantity of AgNPs released from the membrane was evaluated during continuous membrane operation using 2 L pure water. Figure 6 shows the release of Ag element from the Ag/PVDF and Ag-PVDF membrane nanocomposites during deionized water filtration. Figure 6a shows that approximately 52% of the Ag was released from Ag/PVDF membrane nanocomposite and into the filtrate after filtering 2 L water. A significant fraction of the Ag (43.6%) was released from the Ag/PVDF membrane nanocomposite during even the initial stages of filtration, up to 500 mL. On the other hand, the Ag-PVDF membrane nanocomposite did not lose a detectable amount of AgNPs during the entire water filtration process, even though the membrane had a 5-fold greater Ag loading compared to the Ag/PVDF membrane nanocomposite.

The XPS data (see Figure 6b and c) revealed that the peak intensity corresponding to the Ag $3d_{5/2}$ orbital binding energy in the Ag-PVDF membrane nanocomposite was present without a loss of the intensity after filtering 2 L of water. The intensity of the Ag XPS peaks in the Ag/PVDF membrane nanocomposite, by contrast, was markedly reduced, indicating a loss of the AgNPs from the surface of membrane. The stable covalent bond between the AgNPs and the membrane prevented the release of AgNPs from the Ag-PVDF membrane nanocomposite due to the formation of the sulfur−metal covalent interaction.

Biofouling Resistance. Previous studies[17,18,32] have reported that Ag may be released from a Ag/membrane composite as Ag^+ ions, which then act as biocidal agents. These reports concluded that the release of Ag^+ ions is required for realizing high anti-biofouling properties; however, our Ag-

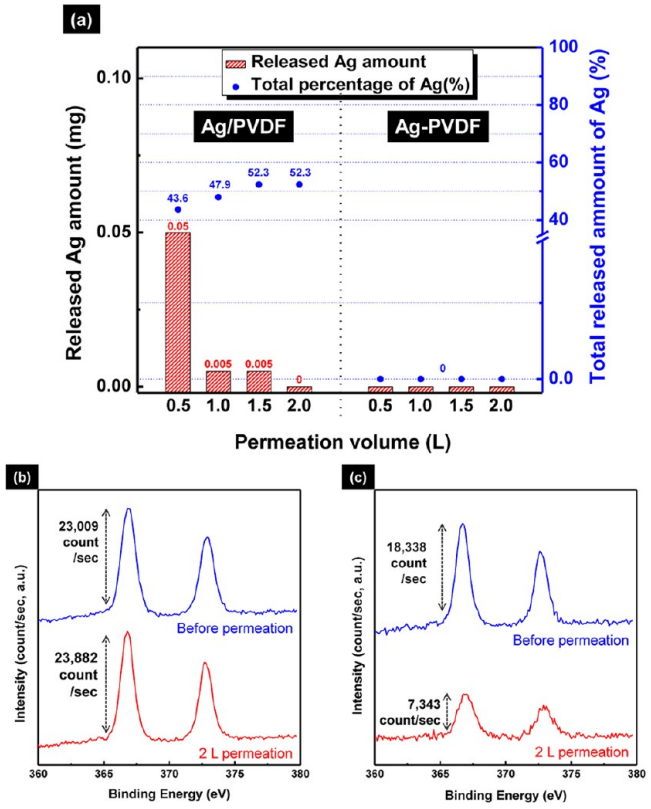

Figure 6. (a) Amount of Ag released into the filtrate from the Ag/PVDF and the Ag-PVDF membrane nanocomposites. XPS spectra of the Ag 3d orbital from (b) the Ag-PVDF and (c) the Ag/PVDF membrane nanocomposites, before and after pure water filtration.

PVDF membrane nanocomposite released no elemental Ag or Ag^+ ions. We next tested the resistance of the Ag-PVDF membrane nanocomposite to biofouling using *E. coli* as a biofoulant. The degree of resistance to biofouling was evaluated by incubating membrane samples in the presence of a stationary phase cell suspension of *E. coli* at 37 °C for 4 h. The cultured membranes were then imaged by FE-SEM to observe the bacteria-adhered membrane surface. As shown in Figure 7, the membrane surface images of the cultured neat and Ag-PVDF membranes were distinctly different. Debris from dead *E. coli* could be observed on the Ag-PVDF membrane nanocomposite surface (Figure 7d–f), whereas intact live *E. coli* were observed on the neat PVDF membrane surface (Figure 7a–c). The assembled AgNPs effectively killed the bacteria on the membrane surface. The strong antibacterial effects of the Ag-PVDF membrane nanocomposite may reduce biofouling of the membrane by suppressing the growth and development of bacteria on the membrane surface. As shown in Figure 8a, the normalized flux through the *E. coli* inoculated neat PVDF and Ag-PVDF membranes decreased continuously due to membrane fouling as the LB broth solution was passed over. However, the normalized flux through the Ag-PVDF membrane nanocomposite was 3 times higher than that of the neat PVDF membrane after filtering the nutrient solution over 25 h. The normalized flux of the neat PVDF membrane was 0.038, whereas the normalized flux of the Ag-PVDF membrane nanocomposite was 0.11. These results were attributed to the suppression of microorganism adhesion and growth due to the biocidal properties of the Ag-PVDF membrane nanocomposite. Surprisingly, the normalized PWP value of the biofouled Ag-PVDF membrane nanocomposite was 0.88 after flushing with DI water. The extent of reversible fouling was calculated to be 74% and the extent of irreversible fouling was 12%. These results suggested that nearly all of the foulants that had attached to the membrane surface had been removed by DI water flushing, and the membrane performance was nearly recovered. On the other hand, the normalized flux through the biofouled neat PVDF membrane after DI water flushing was 0.36. The calculated reversible fouling was 29% and the irreversible fouling was 64%, indicating that the neat PVDF membrane lost much of its functionality to irreversible biofouling. The surfaces of the fouled membranes after the filtration test were observed using FE-SEM (Figure 8c and d). Almost none of the adhered *E. coli* cells remained present on the surface of the Ag-PVDF membrane nanocomposite, whereas many intact *E. coli* cells were observed on the neat PVDF membrane surface. These results show that covalent assembly of AgNPs provides PVDF

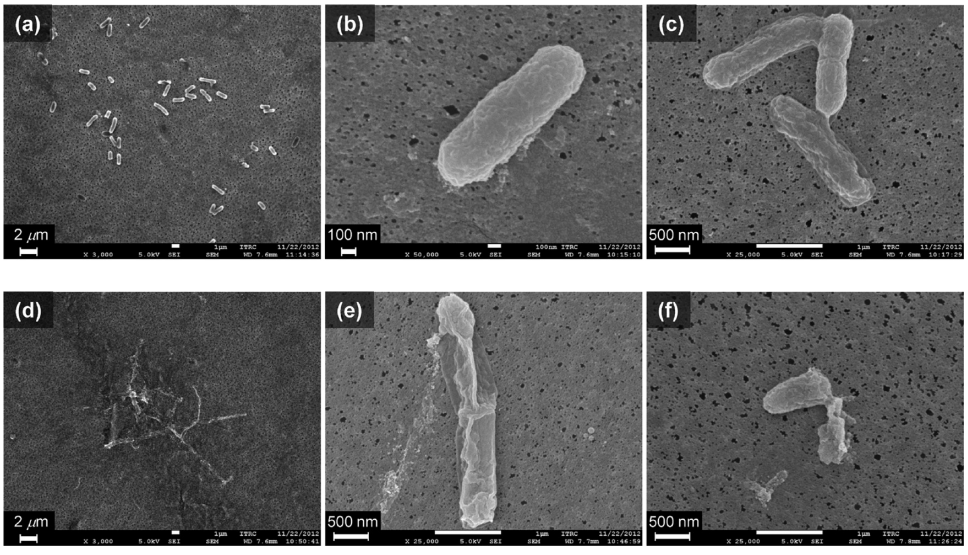

Figure 7. FE-SEM images of the surface adhered *E. coli* on (a–c) the neat PVDF membrane and (d–f) the Ag-PVDF membrane nanocomposite. Both the membranes were incubated with stationary phase of *E. coli* suspension for 4 h at 37 °C.

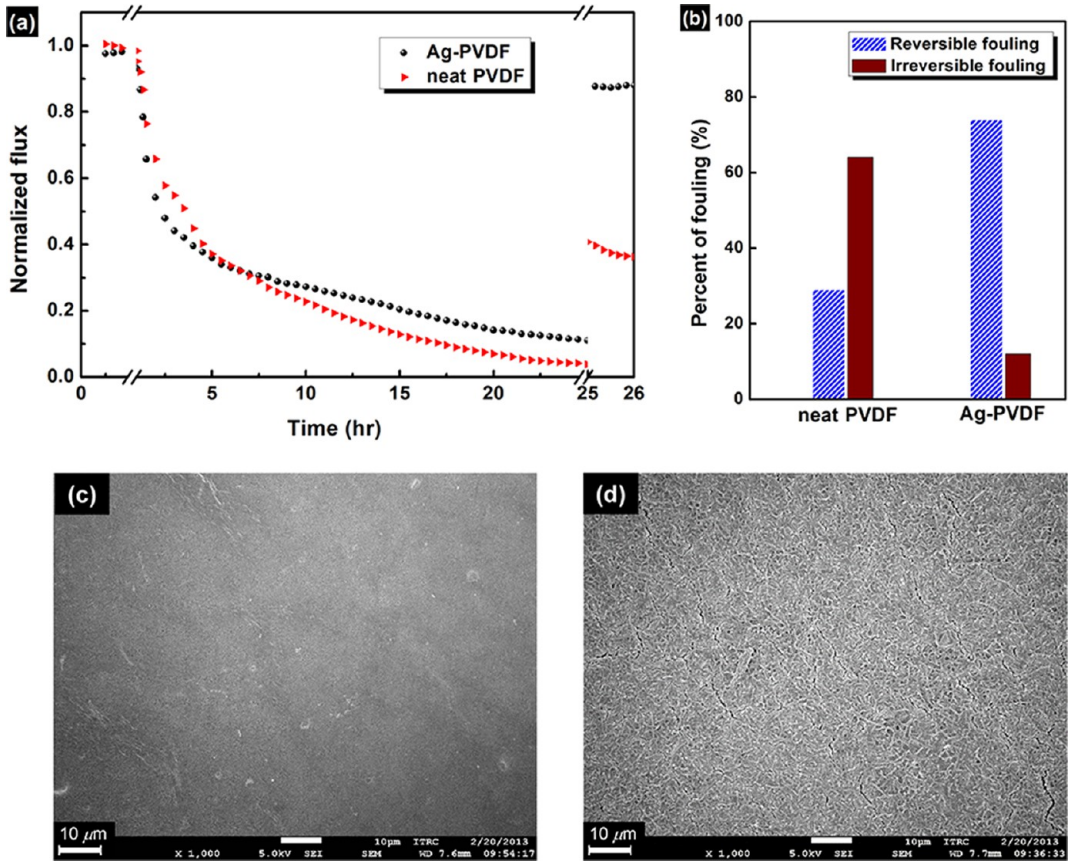

Figure 8. (a) Filtration test of *E. coli* inoculated neat and Ag-PVDF membranes using a synthetic nutrient media feed solution, and (b) calculated percentage of the reversible and the irreversible fouling of the neat PVDF and the Ag-PVDF membranes. FE-SEM images of membrane top surfaces of (c) the neat PVDF and (d) the Ag-PVDF membranes after the filtration test.

membrane with a sustainable anti-biofouling property without released Ag^+ ions. Thus, it is believe that the covalently assembled Ag-PVDF membrane nanocomposite can well be applied to a high performance and ecofriendly water purification system.

CONCLUSIONS

We developed a sustainable anti-biofouling active membrane nanocomposite via the formation of a robust covalent linkage between AgNPs and a PVDF membrane, mediated by a thiol-end functional amphiphilic block copolymer linker. The thiolated amphiphilic linker was prepared and anchored onto the PVDF membrane via hydrophilic−hydrophobic phase separation assembly of the linker during membrane production using a NIPS process, resulting in the formation of a thiolated PVDF membrane. Immersion of the thiolated PVDF membrane in a pH-controlled colloidal AgNP aqueous solution yielded the Ag-PVDF membrane nanocomposite, in which the AgNPs were highly deposited. The membrane morphology and performance were similar to the properties observed in the neat PVDF membrane. ICP-AES and XPS results revealed that the Ag-PVDF membrane nanocomposite displayed excellent binding stability and did not release the Ag from the membrane. In particular, the Ag-PVDF membrane nanocomposite distinctly suppressed the growth of *E. coli* on the membrane surface and showed enhanced and sustainable anti-biofouling properties. These features make the Ag-PVDF membrane nanocomposite quite attractive as an ecofriendly and human-friendly cost-effective water treatment system.

ASSOCIATED CONTENT

Supporting Information

TEM images of the silver nanoparticles. FT-IR spectra of mercaptoacetic acid, polyethylene-*block*-polyethylene glycol, and the thiol-modified polyethylene-*block*-polyethylene glycol copolymer. Photographic image of the Ag-PVDF membrane nanocomposite. SEM images and the EDXS spectra of top and bottom surfaces of the Ag-PVDF membrane nanocomposite. This material is available free of charge via the Internet at http://pubs.acs.org.

AUTHOR INFORMATION

Corresponding Author

*Tel.: +82 2 880 8365. Fax: +82 2 885 1748. E-mail: sykwak@snu.ac.kr.

Author Contributions

‖S.Y.P. and J.W.C.: Equally contributing co-first author.

Notes

The authors declare no competing financial interest.

ACKNOWLEDGMENTS

This work was supported by the Industrial Strategic Technology Development Program funded by the Ministry of Knowledge Economy, Republic of Korea.

REFERENCES

(1) WHO/UNICEF. *Progress on Sanitation and Drinking Water: 2010 update* [Online]; World Health Organization: Geneva and United

Nations Children's Fund: New York, 2010; pp 4−14, http://www.unicef.org/eapro/JMP-2010Final.pdf (accessed Sep 10, 2013).
(2) Rana, D.; Matsuura, T. *Chem. Rev.* **2010**, *110*, 2448−2471.
(3) McDonogh, R.; Schaule, G.; Flemming, H.-C. *J. Membr. Sci.* **1994**, *87*, 199−217.
(4) Drews, A. *J. Membr. Sci.* **2010**, *363*, 1−28.
(5) Hilal, N.; Kochkodan, V.; Al-Khatib, L.; Levadna, T. *Desalination* **2004**, *167*, 293−300.
(6) Yang, H.-L.; Lin, J. C.-T.; Huang, C. *Water Res.* **2009**, *43*, 3777−3786.
(7) Chang, Y.; Ko, C.-Y.; Shih, Y.-J.; Quémener, D.; Deratani, A.; Wei, T.-C.; Wang, D.-M.; Lai, J.-Y. *J. Membr. Sci.* **2009**, *345*, 160−169.
(8) Yang, Y.-F.; Li, Y.; Li, Q.-L.; Wan, L.-S.; Xu, Z.-K. *J. Membr. Sci.* **2010**, *362*, 255−264.
(9) Venault, A.; Chang, Y.; Wang, D.-M.; Lai, J.-Y. *J. Membr. Sci.* **2012**, *423−424*, 53−64.
(10) Liu, C. X.; Zhang, D. R.; He, Y.; Zhao, X. S.; Bai, R. *J. Membr. Sci.* **2010**, *346*, 121−130.
(11) Cen, L.; Neoh, K. G.; Ying, L.; Kang, E. T. *Surf. Interface Anal.* **2004**, *36*, 716−719.
(12) Yu, S.-H.; Mi, F.-L.; Shyu, S.-S.; Tsai, C.-H.; Peng, C.-K.; Lai, J.-Y. *J. Membr. Sci.* **2006**, *276*, 68−80.
(13) Razmjou, A.; Mansouri, J.; Chen, V. *J. Membr. Sci.* **2011**, *378*, 73−84.
(14) Yang, Y.; Zhang, H.; Wang, P.; Zheng, Q.; Li, J. *J. Membr. Sci.* **2007**, *288*, 231−238.
(15) Kim, S. H.; Kwak, S.-Y.; Sohn, B.-H.; Park, T. H. *J. Membr. Sci.* **2003**, *211*, 157−165.
(16) Kwak, S. Y.; Kim, S. H.; Kim, S. S. *Environ. Sci. Technol.* **2001**, *35*, 2388−2394.
(17) Zodrow, K.; Brunet, L.; Mahendra, S.; Li, D.; Zhang, A.; Li, Q.; Alvarez, P. J. J. *Water Res.* **2009**, *43*, 715−723.
(18) Nisola, G. M.; Park, J. S.; Beltran, A. B.; Chung, W. J. *RSC Adv.* **2012**, *2*, 2439−2448.
(19) Zhang, M.; Zhang, K.; De Gusseme, B.; Verstraete, W. *Water Res.* **2012**, *46*, 2077−2087.
(20) Taurozzi, J. S.; Arul, H.; Bosak, V. Z.; Burban, A. F.; Voice, T. C.; Bruening, M. L.; Tarabara, V. V. *J. Membr. Sci.* **2008**, *325*, 58−68.
(21) Kim, Y.; Rana, D.; Matsuura, T.; Chung, W. J. *Chem. Commun.* **2012**, *48*, 693−695.
(22) Reich, L.; Stivala, S. S. *J. Appl. Polym. Sci.* **1969**, *13*, 977−988.
(23) Ostuni, E.; Chapman, R. G.; Holmlin, R. E.; Takayama, S.; Whitesides, G. M. *Langmuir* **2001**, *17*, 5605−5620.
(24) Li, Q.; Mahendra, S.; Lyon, D. Y.; Brunet, L.; Liga, M. V.; Li, D.; Alvarez, P. J. J. *Water Res.* **2008**, *42*, 4591−4602.
(25) Davies, R. L.; Etris, S. F. *Catal. Today* **1997**, *36*, 107−114.
(26) Choi, O.; Deng, K. K.; Kim, N.-J.; Ross, L., Jr.; Surampalli, R. Y.; Hu, Z. *Water Res.* **2008**, *42*, 3066−3074.
(27) Marius, S.; Lucian, H.; Marius, M.; Daniela, P.; Irina, G.; Romeo-Iulian, O.; Simona, D.; Viorel, M. *J. Mater. Sci.: Mater. Med.* **2011**, *22*, 789−796.
(28) Samberg, M. E.; Orndorff, P. E.; Monteiro-Riviere, N. A. *Nanotoxicology* **2011**, *5*, 244−253.
(29) AshaRani, P. V.; Mun, G. L. K.; Hande, M. P.; Valiyaveettil, S. *ACS Nano* **2009**, *3*, 279−290.
(30) Larese, F. F.; D'Agostin, F.; Crosera, M.; Adami, G.; Renzi, N.; Bovenzi, M.; Maina, G. *Toxicology* **2009**, *255*, 33−37.
(31) Yang, Z.; Liu, Z. W.; Allaker, R. P.; Reip, P.; Oxford, J.; Ahmad, Z.; Ren, G. *J. R. Soc., Interface* **2010**, *7*, S411−S422.
(32) Mauter, M. S.; Wang, Y.; Okemgbo, K. C.; Osuji, C. O.; Giannelis, E. P.; Elimelech, M. *ACS Appl. Mater. Interfaces* **2011**, *3*, 2861−2868.
(33) Park, S. Y.; Chung, J. W.; Priestley, R. D.; Kwak, S. Y. *Cellulose* **2012**, *19*, 2141−2151.
(34) Lee, G. J.; Shin, S. I.; Kim, Y. C.; Oh, S. G. *Mater. Chem. Phys.* **2004**, *84*, 197−204.
(35) Schnippering, M.; Carrara, M.; Foelske, A.; Kotz, R.; Fermin, D. J. *Phys. Chem. Chem. Phys.* **2007**, *9*, 725−730.
(36) Wang, H.; Lee, J.-K.; Moursi, A. M.; Anderson, D.; Winnard, P.; Powell, H.; Lannutti, J. *J. Biomed. Mater. Res., Part A* **2004**, *68A*, 61−70.
(37) Pearson, R. G. *J. Am. Chem. Soc.* **1963**, *85*, 3533−3539.
(38) Hiramatsu, H.; Osterloh, F. E. *Chem. Mater.* **2004**, *16*, 2509−2511.